ADVANCED ENERGY MATERIALS
www.advenergymat.de

A Water-Proof Triboelectric–Electromagnetic Hybrid Generator for Energy Harvesting in Harsh Environments

*Hengyu Guo, Zhen Wen, Yunlong Zi, Min-Hsin Yeh, Jie Wang, Liping Zhu, Chenguo Hu, and Zhong Lin Wang**

Packaging is a critical aspect of triboelectric nanogenerators (TENG) toward practical applications, since the performance of TENG is greatly affected by environmental conditions such as humidity. A waterproof triboelectric–electromagnetic hybrid generator (WPHG) for harvesting mechanical energy in harsh environments is reported. Since the mechanical transmission from the external mechanical source to the TENG is through a noncontact force between the paired magnets, a fully isolated packaging of TENG part can be easily achieved. At the same time, combining with metal coils, these magnets can be fabricated to be electromagnetic generators (EMG). The characteristics and advantages of outputs from both TENG and EMG are systematically studied and compared to each other. By using transformers and full-wave rectifiers, 2.3 mA for total short-circuit current and 5 V for open-circuit voltage are obtained for WPHG under a rotation speed of 1600 rpm, and it can charge a supercapacitor (20 mF) to 1 V in 22s. Finally, the WPHG is demonstrated to harvest wind energy in the rainy condition and water-flow energy under water. The reported WPHG renders an effective and sustainable technology for ambient mechanical energy harvesting in harsh environments. Solid progress in both the packaging of TENG and the practical applications of the hybrid generator toward practical power source and self-powered systems is presented.

1. Introduction

Due to the challenges of energy crisis and related environmental issues, scavenging renewable energy, such as solar energy, hydropower, and wind power from the ambient environment, has become mandatory for the sustainable development of modern society. Recently, nanogenerators[1–7] have been invented to power electronic devices by harvesting energy from the environment. Among them, based on the coupling of the triboelectrification effect and electrostatic induction, triboelectric nanogenerators (TENG) have shown advantages of light weight, extreme low cost, and simplicity in fabrication,[1,3,8–10] which can be used to harvest almost all forms of mechanical energies, such as vibrations,[11–16] airflow,[17–19] water waves,[20–22] rotation,[23–25] and even acoustic energy.[26,27] However, it has been demonstrated that the triboelectrification effect can be greatly affected by the environmental conditions, such as humidity and surface adsorption layers.[4,28,29] Thus, packaging plays a critical role for TENG toward broader practical applications especially for in vivo medical purposes and under water. Due to the presence of the mechanical triggering, packaging of TENG while preserving the ability of the moveable part to be driven by the external mechanical triggering is important for retaining and improving its performance. Previously, Yang et al. had demonstrated a fully enclosed packaged TENG to be used in water and harsh environments. However, this approach just provides a direct packaging on TENG without considerations on the mechanical transmission. Therefore, the motion in the ambient environment cannot be effectively transferred to the motion of the working components in TENG, especially for sliding mode TENG or free-standing-triboelectric-layer mode TENG. A packaging strategy that is applicable for a large variety of TENGs is required.

At the same time, TENG has been hybridized with various other energy harvesters to simultaneously collecting energy from various sources.[30–32] Among these hybrid generators, the one consisting of TENG and electromagnetic generator (EMG) has been developed to effectively harvest mechanical energy.[19,30,33,34] In them, a rotation-based hybrid generator has been reported to produce a large output that can sustainably drive a commercial

H. Guo, Z. Wen, Dr. Y. Zi, Dr. M.-H. Yeh, Dr. J. Wang, Prof. Z. L. Wang
School of Materials Science and Engineering
Georgia Institute of Technology
Atlanta, GA 30332-0245, USA
E-mail: zhong.wang@mse.gatech.edu
H. Guo, Prof. C. Hu
Department of Applied Physics
Chongqing University
Chongqing 400044, China
Z. Wen, Prof. L. Zhu
State Key Laboratory of Silicon Materials
School of Materials Science & Engineering
Cyrus Tang Center for Sensor Materials and Applications
Zhejiang University
Hangzhou, Zhejiang 310027, China
Prof. Z. L. Wang
Beijing Institute of Nanoenergy and Nanosystems
Chinese Academy of Sciences
Beijing 100083, China

DOI: 10.1002/aenm.201501593

globe light with an intensity of illumination up to 1700 lx.[34] However, for this kind hybrid generator, the influences of parameters on both TENG and EMG have not been well studied, and the two generators have not been systematically compared with each other. A more systematic and complete research to reveal the advantages and complementary characteristics of the outputs for both generators in the hybrid mode is required.

Herein, we present a waterproof triboelectric–electromagnetic hybrid generator (WPHG) for harvesting energy in harsh environments. We design a strategy to indirectly drive the movable part of the TENG through the noncontact attractive forces between pairs of magnets. With this design, the TENG part can be fully isolated from the external environment through packaging, and the EMG can be easily hybridized on the device. In this work, a systematic study of the influences of the designed parameters, including the segmentation of the TENG and the arrangement of the coils, on the electrical outputs of the WPHG are performed experimentally. Compared with EMG, TENG can produce a stable voltage to power commercial electronic device even under a low rotation speed. TENG and EMG play complementary roles in output performance so that WPHG can deliver usable outputs under a large range of rotation speeds. With the utilization of transformers and rectifiers, the output resistances of TENG and EMG with very different characteristics are hybridized, which can charge a supercapacitor (20 mF) to 1 V in 22 s. Finally, the WPHG is demonstrated to harvest the energy in harsh environment, such as wind energy in the rainy condition and the water-flow energy under water. This work represents a solid progress in both the packaging of TENG and the practical applications of the hybrid generator toward the sustainable power source for electronics.

2. Results and Discussion

The device structure of the multilayered WPHG is schematically illustrated in **Figure 1**a, which mainly consists of two parts: TENG and EMG. This rotational sliding freestanding-triboelectric-layer mode TENG contains a stator and a rotator (the moveable part).[25] A nummular acrylic sheet with a diameter of 100 mm was deposited by complementary radially patterned copper electrodes (segments of 24) before covering an fluorinated ethylene propylene (FEP) thin film (50 μm in thickness) as the stator. Nanowires with ≈100 nm in diameter and ≈1 μm in length were fabricated on the FEP film as one triboelectric layer to enhance the surface charge density,[35–38] as shown in Figure 1d. The rotator of TENG (85 mm in diameter) was made of a nummular sponge sheet, which was stuck to one side of an acrylic sheet. Copper thin film with the pattern same as that of one set of the complementary electrodes was deposited on the sponge as the other triboelectric layer. Six magnets with the same magnetic polarization were evenly fixed on the other side of the acrylic sheet around the center. Similarly, the EMG part also consists of a stator and a rotator. The stator part of EMG was fabricated by an acrylic sheet (100 mm in diameter) with six synclastic twined coils embedded inside. To prepare the rotator of the EMG, six magnets were fixed on an acrylic sheet (85 mm in diameter). Both the magnets and coils on EMG were aligned to the magnets on the rotator of TENG one-by-one. The attractive forces were formed between the two sets of magnets, and the rotator of TENG can be driven by operating the rotator of EMG without direct contact, which is the key strategy to achieve waterproof packaging of the TENG. The linkage mechanism[39,40] and the design of the EMG part are shown in Figure S1 in the Supporting Information. The strategies to further improve the output performances of TENG[25] and EMG[39,41,42] are discussed in Supporting Information, and the reported highest output of TENG[43] and EMG[44] is also listed in the Supporting Information. By using the encapsulation ring between the stator of TENG and EMG, the TENG part can be fully isolated from the external environment. Figure 1b,c shows the photographs of the EMG part and TENG part. Detailed information about fabrication can be found in the Section 4.

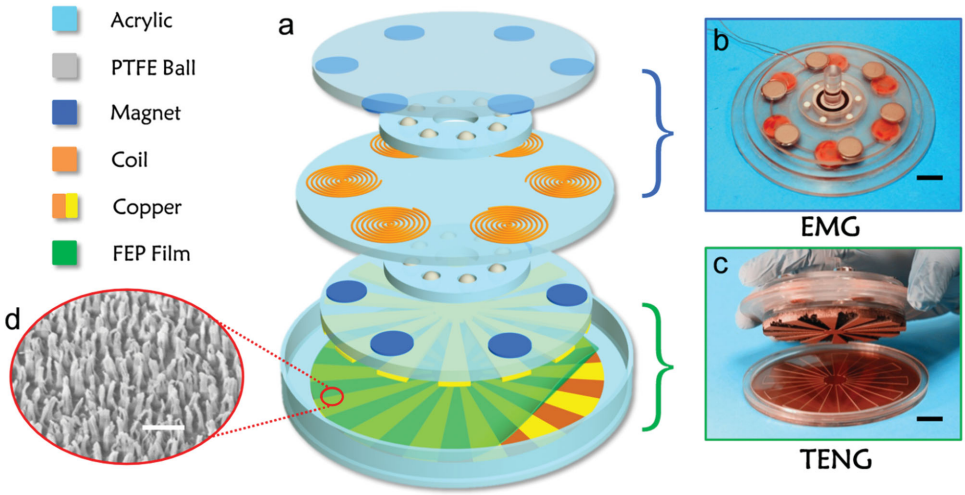

Figure 1. Structure design of the WPHG. a) A schematic illustrations of the functional components of WPHG, which mainly consists of two parts, a free-standing-triboelectric-layer mode (TENG) and an EMG. A photograph of b) an as-fabricated EMG and c) an as-fabricated TENG (both the scale bar are 1 cm). d) A SEM image of the FEP polymer nanowires (scale bar, 500 nm).

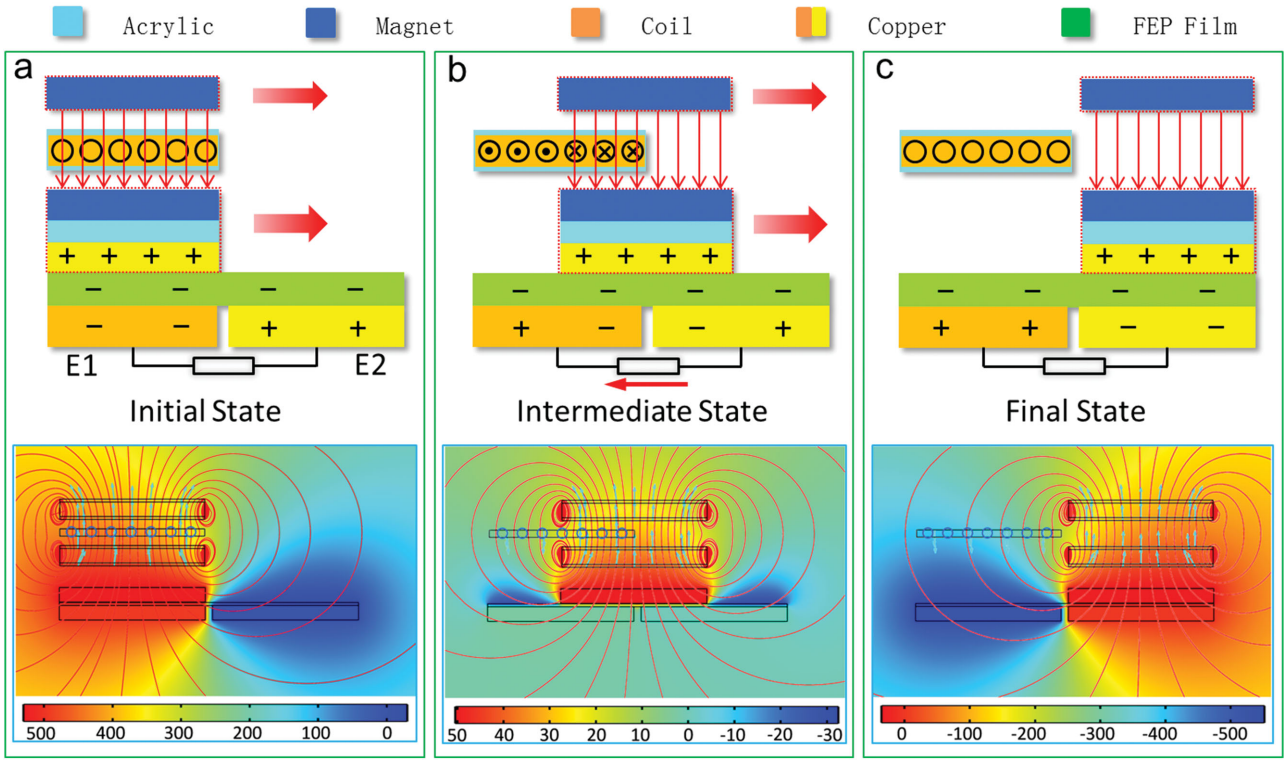

Figure 2. Schematic diagrams of the working principle of the hybridized EMG and TENG. The diagrams illustrate the cross-sectional schematic of WPHG in a half cycle, current, and charge distribution in short-circuit condition (upper), magnetic flux (upper and lower), and potential distribution simulated by COMSOL in open-circuit condition (lower), respectively, in a) the initial state, b) the intermediate state, and c) the final state.

The electricity generation of the waterproof hybrid generator can be divided into two parts: the part from TENG and the part from EMG, as schematically depicted in **Figure 2**. Here, the working mechanisms were explained by schematic illustrations of current and charge distribution (upper) in short-circuit condition, magnetic flux (upper and lower), and potential distribution (lower) in open-circuit condition simulated by COMSOL Multiphysics software. We define the initial state (Figure 2a) and the final state (Figure 2c) as the states when the triboelectric layer on the rotator aligned with electrode 1 (E1) and electrode 2 (E2), respectively. At the same time, the magnets in the two states are fully aligned and misaligned with the coils, respectively, to synchronize the outputs of TENG and EMG. During rotation of the rotators, triboelectrification occurs and equal amount of negative and positive charges are generated on the FEP surface and the copper surface, respectively, due to the difference of the electron affinity between copper and FEP.[4,45] In the initial state, owing to electrostatic induction, the negative and positive charges are induced on E1 and E2, respectively, to screen the electric field. And then during rotation, the potential difference between electrodes will be built and the negative charges on E1 will transfer to E2 through the external circuit to maintain the equilibrium state, until it reaches the final state. Because of the symmetric structure, the rotation beyond the final state until the next initial state induces the reversed potential difference and hence the current flows in the opposite direction. Simultaneously, when the rotator part of EMG spins from the initial state to the final state, the magnetic flux crossing the coil decreases, which induces current in the coil to generate a magnetic field which can impede the decrease of the magnetic flux due to the Lenz's law; similarly, the rotation between the final state and the next initial state induces the current flow in the reversed direction.

For TENG, according to our previous work, the amplitudes of open-circuit voltage and short-circuit current can be represented as[46,47]

$$V_{oc}^{TE} = \frac{\sigma S}{C} \tag{1}$$

$$I_{sc}^{TE} = \frac{n}{\pi}\frac{\sigma}{2} S\omega \tag{2}$$

where σ is the charge density on FEP surface, S is the area of one electrode, C is the capacitance between the two electrodes, n is the segments' number of the rotator, and ω is the rotational angular velocity. Referring to Equations (1) and (2), by increasing the segments' number or the rotation speed, both the amplitude and the output frequency of I_{sc}^{TE} will increase proportionally; in the meanwhile, the V_{oc}^{TE} will almost keep constant. In order to study the effects of these two parameters on the output performance of TENG (here the diameter of TENG is 60 mm), a group of tests were carried out. **Figure 3**a,b shows the dependence of the short-circuit current and open-circuit voltage of TENG on the segments' number (from 2 to 12) under 600 rpm rotation speed, from which we can observe that I_{sc}^{TE}

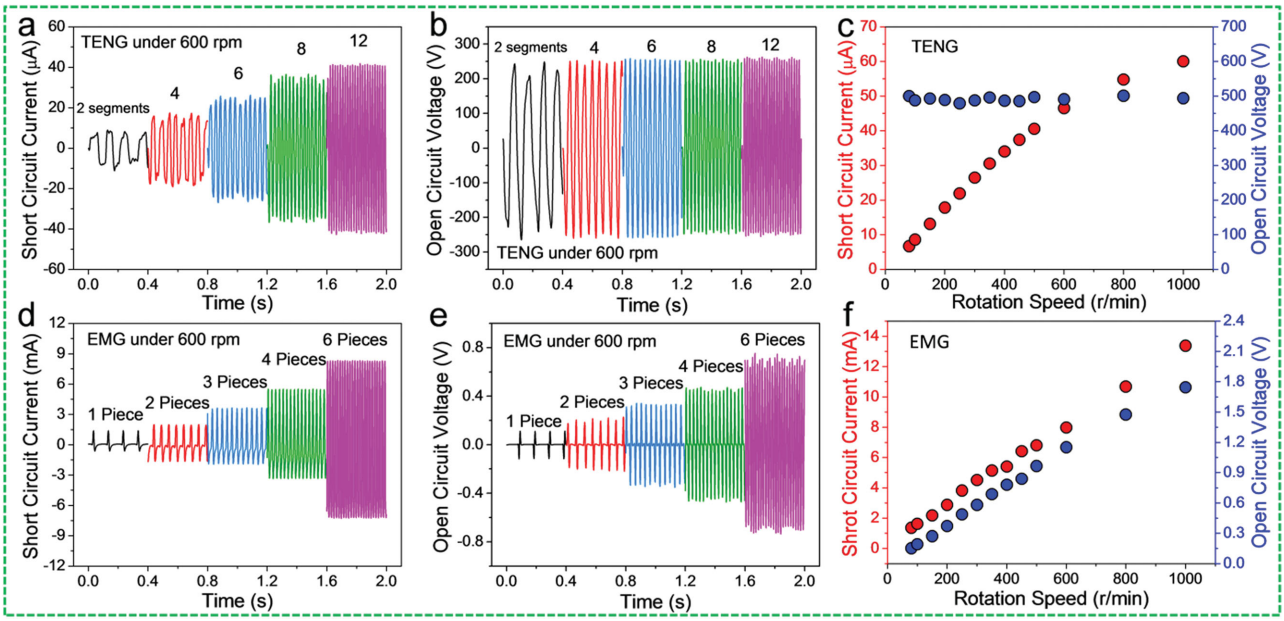

Figure 3. The electrical performance dependence of the TENG and EMG on the parameters. a) The short-circuit current and b) the open-circuit voltage of the TENG with different number of segments. c) The amplitudes of short-circuit current and open-circuit voltage of the TENG with the segmentation of 12 under various rotation speed. d) The short-circuit current and e) the open-circuit voltage of the EMG with different number of coil–magnet pairs. f) The amplitudes of short-circuit current and open-circuit voltage of the EMG with the coil–magnet pairs' number of 6 under various rotation speed.

raises linearly from ≈10 to ≈40 μA with the segments' number increase, while V_{oc}^{TE} stays almost constant (≈500 V). At the same time the frequencies of both short-circuit current and open-circuit voltage increase. The I_{sc}^{TE} and V_{oc}^{TE} with different rotation speeds (segments' number of 12) are plotted in Figure 3c, which shows the same tendency as that of the change by segments' number.

For EMG, according to the Faraday's law, the open-circuit voltage and short-circuit current can be expressed as

$$V_{oc}^{EM} = -N\frac{d\Phi_B}{dt} \tag{3}$$

$$I_{sc}^{EM} = \frac{V_{oc}^{EM}}{R} \tag{4}$$

in which B is the magnetic field, Φ_B is the total magnetic flux in each coil and N is the number of the coil–magnet pairs. R represents the internal resistance of the coil. Apparently the variation rate of the magnetic flux is related to the rotation speed. From Equations (3) and (4), by increasing either the number of the coil–magnet pairs or the rotation speed, both the amplitude and the frequency of V_{oc}^{EM} and I_{sc}^{EM} increase. In this work, a group of experiments were carried out for systematically investigating the output performance of EMG (100 turns for each coil). Figure 3d,e shows the dependence of the short-circuit current and open-circuit voltage of EMG under 600 rpm rotation speed on the number of coil–magnet pairs (from 1 to 6), from which we can observe that both of the amplitudes and the frequency raise linearly from ≈1.3 mA, ≈0.2 V, and 10 Hz to ≈8 mA, ≈1.4 V, and 60 Hz with the number increasing. By comparing Figure 3a,b with d,e, based on our rational design, the outputs from TENG and the EMG can be in phase. From Figure 3c,f we noticed that, under a low rotation speed, the EMG can only supply very low voltage which cannot be used for powering electronic devices; as a comparison, the voltage from TENG can be always maintained at a high level, which is ready for use as an instantaneous power source. This feature of TENG will be advantageous for harvesting low-frequency mechanical energy which is more common in the ambient environment. As a power source, working at the matched resistance can maximize the output power. As we know, the characteristics of TENG and EMG are quite different: under the constant rotation speed, TENG can be regarded as a current source with a large output resistance, while the EMG is equivalent to a voltage source with a small internal resistance.[48] To achieve the maximized output power and the matched resistances of TENG (segments of 12) and EMG (six magnets and coils), the relationship between the electric output and the external load resistance under the rotation speed of 1600 rpm are recorded and shown in Figure S2a,b in the Supporting Information. The obtained maximum output power is 7 mW at a load resistance of 10 MΩ for TENG and 4.5 mW at a load resistance of 60 Ω for EMG. The six orders of magnitude difference makes the TENG and the EMG unable to charge the same external load at the maximized power outputs simultaneously. To solve this problem, transformers were used for adjusting the output resistances of TENG and EMG. **Figure 4**a,b shows the measured output voltages and powers of both TENG and EMG under the different external load resistances. The matched resistances of TENG and EMG were adjusted to 1 and 1.2 KΩ, respectively; and besides, the open-circuit voltages were both adjusted to be around 5 V. Meanwhile, the short-circuit currents of TENG and EMG changed from ≈100 μA and ≈15 mA to ≈1.5 and 1.2 mA, respectively. The open-circuit voltage and

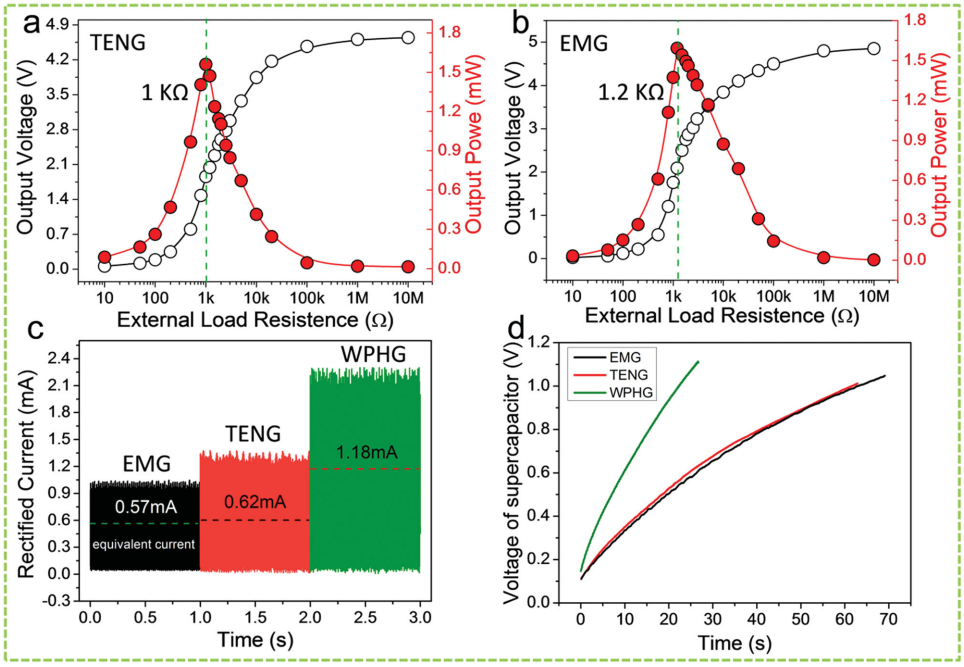

Figure 4. The characters of TENG and EMG after impedance matching and the performance of the hybrid generator for charging a supercapacitor. The dependence of the output voltage and power on the external load resistance of the a) TENG and b) EMG after using the transformer (rotation speed of 1600 rpm). The output resistances of TENG and EMG were adjusted to the same magnitude by transformers. c) The rectified short-circuit current of EMG, TENG, and hybrid generator. The current values indicate corresponding average currents. d) The charging curves of EMG, TENG, and WPHG.

short-circuit current curves of TENG and EMG before and after using transformers are shown in Figure S3 and Figure S4 in the Supporting Information, respectively. For practical applications and energy storage in capacitors or batteries, the rectifiers are used for converting the AC signal of the WPHG to DC signal. With transformers used as described above, the rectified short-circuit current and open-circuit voltage of TENG, EMG, and WPHG are shown in Figure 4c and Figure S2c in the Supporting Information, respectively, which indicate that the current of the WPHG is added up to ≈2.3 mA in peak value and 1.18 mA in average value while connecting TENG (≈1.3 mA in peak value and 0.62 mA in average value) and EMG (≈1.0 mA in peak value and 0.57 mA in average value) in parallel, and the voltage amplitudes of them are kept at almost ≈5 V. The average current values are calculated by using equation $\overline{I} = \frac{\int_0^T I(t)\mathrm{d}t}{T}$. This WPHG output is demonstrated to charge a 20 mF supercapacitor. The charging voltage curves of the supercapacitor of TENG, EMG, and WPHG are depicted in Figure 4d, with the electric circuit as shown in Figure S2d in the Supporting Information. From Figure 4d, the supercapacitor can be charged to be 1 V in ≈22 s by WPHG. The beginning charging rates for TENG, EMG, and WPHG are extracted from the plots as 29.49, 27.64, and 58.05 mV s^{-1}, respectively. Consequently, we can calculate the equivalent charging currents of TENG, EMG, and WPHG as 0.590, 0.553, and 1.161 mA, respectively.[32] These results are consistent with the average short-circuit currents as calculated above. Through comparing the charging rates and currents of the TENG, EMG, and WPHG, it is indicated that the outputs of TENG and EMG are able to be directly added by the hybridization process.

The utilization of the magnet pairs for indirect noncontact mechanical transmission enables the fully enclosed packaging of the TENG. To demonstrate the capability of the WPHG as a practical power source for harvesting mechanical energy in harsh environments, it is directly integrated with commercial LED bulbs without using any storage or power regulation units. Several yellow LED bulbs, making up the word "MEG," are connected to the EMG in parallel. And several green LED bulbs are connected to the TENG in series, which constitute the word "TENG," as shown in **Figure 5**a. The circuit diagrams of the two lighting systems are shown in Figure S5 in the Supporting Information. The output current curves for TENG with and without packaging in the dry and under-water conditions and the 7 d long-term stability of the WPHG sealed by epoxy are measured as shown in Figures S6 and S7 in the Supporting Information. We observe that the TENG with packaging can work in both dry and under-water conditions with similar outputs, while the TENG without packaging can only work in the dry condition, and it has nearly no outputs in the under-water condition, the long-term stability shows a perfect fully enclosed TENG part using this packaging method. For practical application, a wind wheel is installed on the WPHG with packaged TENG to harvest wind energy. As wind passes by, the wind wheel starts to rotate and drive the WPHG, which is capable of lighting up the "MEG" and "TENG" LEDs simultaneously. Even in a rainy condition, the device can still work without any influence from the water drops, as displayed in Figure 5b and Movie S1 in the Supporting Information. After that, we deployed a water wheel onto the WPHG instead of the wind wheel for harvesting water-flow energy under water, as illustrated in Figure 5c. For

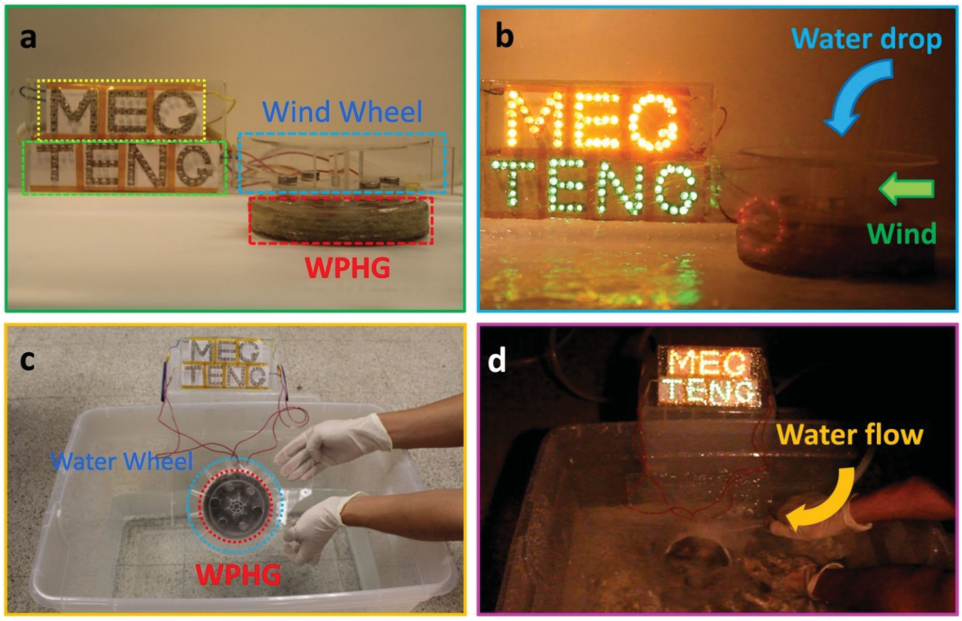

Figure 5. Demonstrations of the water-proof hybrid generator as a practical power source. WPHG was used for harvesting wind energy under simulated rainy condition a) before working and b) after working. WPHG was used for harvesting water-flow energy in the water c) before working and d) after working.

an experimental demonstration, here we employed a homemade water tank to simulate real under-water environment. As shown in Figure 5d and Movie S2 in the Supporting Information, the WPHG is immersed into the water. When water flows through, the water wheel rotates and drives the WPHG to light the LEDs. These results demonstrated the successful fully enclosed packaging of the TENG. And furthermore, this strategy for packaging can also be applied on all the modes of TENG, which makes a solid step for advancing practical applications of TENG technology.

3. Conclusion

In summary, we have demonstrated a waterproof triboelectric–electromagnetic hybrid generator for harvesting mechanical energy in the harsh environment. By creatively utilizing the interactions between pairs of magnets as the noncontact mechanical transmission forces, the fully enclosed packaging of TENG can be easily achieved. Systematic study of the influences of the designed parameters, including the segment's number of the TENG, the rotation speed, and the arrangement of the coils, on the electrical outputs of the WPHG were performed experimentally. Compared with EMG, TENG can produce a stable voltage to power commercial electronic device even under a low rotation speed. By using the transformers and rectifiers, the hybrid outputs of 2.3 mA in short-circuit current and 5 V in open-circuit voltage are obtained for WPHG under a rotation speed of 1600 rpm, which can charge a supercapacitor (20 mF) to 1 V in 22 s. Finally, the WPHG are demonstrated to harvest wind energy in a rainy day and water-flow energy under water to directly power tens of commercial LEDs. The WPHG renders an effective and sustainable technology for ambient mechanical energy harvesting. This work is a solid step on packaging of TENG as well as TENG-based hybrid generator toward practical power source and self-powered systems.

4. Experimental Section

Fabrication of Nanowires Array on FEP Surface: Typically, a 50 μm thick FEP thin film (American Durafilm) was cleaned with isopropyl alcohol and deionized water, and then blown dry with compressed nitrogen gas. Using a DC sputter (Unifilm Sputter), a 10 nm thick layer of Au was coated onto the FEP film as a mask for creating the polymer nanowires array. Au-coated FEP was put into inductively coupled plasma (ICP) chamber, and O_2, Ar, and CF_4 gases were introduced at flow rates of 10.0, 15.0, and 30.0 sccm, respectively. One power source of 400 W was used to generate a large density of plasma and another power source of 100 W was used to accelerate plasma ions toward the FEP surface. The ICP reactive ion etching was then performed for 10 min. The surface morphology of the FEP thin film was characterized by field emission scanning electron microscopy (Hitachi SU-8010).

Fabrication of the TENG Part: The TENG mainly consists of two parts: a stator and a rotator. For the stator, acrylic sheet with thickness of 3 mm was shaped by a laser cutter (PLS6.75, Universal Laser Systems) to form a disk substrate (100 mm). Then, electrodes with complementary patterns had been deposited onto the substrate by pulsed vapor deposition (PVD). And the copper electrodes were separated by laser-cutter-defined fine trenches in between. Two lead wires were connected respectively to the two sets of electrodes. The as-prepared FEP film was aligned onto the substrate as one of the triboelectric layer. For the rotator, a nummular sponge sheet (85 mm in diameter) was stuck to one side of an acrylic sheet (85 mm in diameter), the sponge was deposited with copper layer as the tribomaterial and had the same pattern as that of one electrode. The soft sponge foam was acting as a buffer layer to ensure an intimate contact between the two. Six NdFeB permanent disc magnets with a diameter of 12 mm and a thick of 3 mm with the same side of magnetic pole were evenly arranged and fixed on the other side of the acrylic sheet around the center.

Fabrication of an EMG: The EMG also mainly consists of two parts: the stator and the rotator. For the stator, an acrylic sheet of 100 mm in diameter and 3 mm in thickness was used as the substrate. Six grooves of 2 mm in depth were cut on one side of the substrate aligning to the six magnets on the rotator of TENG. And six coils (200 turns for each) were embedded in the grooves before sealing by an acrylic sheet of 100 mm in diameter and 1 mm in thickness. For the rotator, six NdFeB permanent disc magnets with a diameter of 12 mm and a thick of 3 mm with the same side of magnetic pole were aligned to the magnets on the rotator of TENG and fixed on one side of an acrylic sheet of 85 mm in diameter and 3 mm in thickness. In order to reduce the resistance between each part, lubricating balls and bearings were used for connecting the rotator of TENG, the stator and rotator of EMG.

Assembling of the WPHG: Several acrylic rings (outer diameter of 100 mm and inner diameter of 90 mm) were used for forming the waterproof wall of the TENG part and connecting the stator parts of TENG and EMG. In order to largely reduce the mechanical resistance, two homemade lubricating bearings consisting of several PTEF balls (3 mm in diameter) and an acrylic ring were used for connecting the rotator part of TENG, the stator part of EMG, and the rotator part of EMG.

Electrical Measurement: The output voltage signal of the WPHG via a voltage preamplifier (Keithley 6514 System Electrometer) and the output current signal by a low-noise current preamplifier (Stanford Research System SR570) were acquired. The software platform was constructed based on LabVIEW, which was capable of realizing real-time data acquisition control and analysis.

Supporting Information

Supporting Information is available from the Wiley Online Library or from the author.

Acknowledgements

H.G., Z.W., and Y.Z. contributed equally to this work. Research was supported by National Science Foundation (DMR-1505319) and the Chinese Scholars Council.

Received: August 9, 2015
Revised: October 21, 2015
Published online: December 23, 2015

[1] F.-R. Fan, Z.-Q. Tian, Z. Lin Wang, *Nano Energy* **2012**, *1*, 328.
[2] Y. Hu, Z. L. Wang, *Nano Energy* **2015**, *14*, 3.
[3] Z. L. Wang, *ACS Nano* **2013**, *7*, 9533.
[4] Z. L. Wang, *Faraday Discuss.* **2014**, *176*, 447.
[5] Z. L. Wang, J. Chen, L. Lin, *Energy Environ. Sci.* **2015**, *8*, 2250.
[6] Z. L. Wang, J. Song, *Science* **2006**, *312*, 242.
[7] X.-S. Zhang, M.-D. Han, R.-X. Wang, B. Meng, F.-Y. Zhu, X.-M. Sun, W. Hu, W. Wang, Z.-H. Li, H.-X. Zhang, *Nano Energy* **2014**, *4*, 123.
[8] S. Kim, M. K. Gupta, K. Y. Lee, A. Sohn, T. Y. Kim, K.-S. Shin, D. Kim, S. K. Kim, K. H. Lee, H.-J. Shin, D.-W. Kim, S.-W. Kim, *Adv. Mater.* **2014**, *26*, 3918.
[9] K. Y. Lee, J. Chun, J. H. Lee, K. N. Kim, N. R. Kang, J. Y. Kim, M. H. Kim, K. S. Shin, M. K. Gupta, J. M. Baik, *Adv. Mater.* **2014**, *26*, 5037.
[10] J. Zhong, Q. Zhong, F. Fan, Y. Zhang, S. Wang, B. Hu, Z. L. Wang, J. Zhou, *Nano Energy* **2013**, *2*, 491.
[11] J. Chen, G. Zhu, W. Yang, Q. Jing, P. Bai, Y. Yang, T.-C. Hou, Z. L. Wang, *Adv. Mater.* **2013**, *25*, 6094.
[12] G. Liu, Q. Leng, J. Lian, H. Guo, X. Yi, C. Hu, *ACS Appl. Mater. Interfaces* **2015**, *7*, 1275.
[13] J. Yang, J. Chen, Y. Yang, H. Zhang, W. Yang, P. Bai, Y. Su, Z. L. Wang, *Adv. Energy Mater.* **2014**, *4*, 1301322.
[14] W. Yang, J. Chen, Q. Jing, J. Yang, X. Wen, Y. Su, G. Zhu, P. Bai, Z. L. Wang, *Adv. Funct. Mater.* **2014**, *24*, 4090.
[15] W. Tang, B. Meng, H. X. Zhang, *Nano Energy* **2013**, *2*, 1164.
[16] X.-S. Zhang, M.-D. Han, R.-X. Wang, F.-Y. Zhu, Z.-H. Li, W. Wang, H.-X. Zhang, *Nano Letters* **2013**, *13*, 1168.
[17] J. Bae, J. Lee, S. Kim, J. Ha, B.-S. Lee, Y. Park, C. Choong, J.-B. Kim, Z. L. Wang, H.-Y. Kim, J.-J. Park, U. I. Chung, *Nat. Commun.* **2014**, *5*, 4929.
[18] H. Guo, X. He, J. Zhong, Q. Zhong, Q. Leng, C. Hu, J. Chen, L. Tian, Y. Xi, J. Zhou, *J. Mater. Chem. A* **2014**, *2*, 2079.
[19] X. Wang, S. Wang, Y. Yang, Z. L. Wang, *ACS Nano* **2015**, *9*, 4553.
[20] J. Chen, J. Yang, Z. Li, X. Fan, Y. Zi, Q. Jing, H. Guo, Z. Wen, K. C. Pradel, S. Niu, Z. L. Wang, *ACS Nano* **2015**, *9*, 3324.
[21] Y. Su, X. Wen, G. Zhu, J. Yang, J. Chen, P. Bai, Z. Wu, Y. Jiang, Z. Lin Wang, *Nano Energy* **2014**, *9*, 186.
[22] Y. Yang, H. Zhang, R. Liu, X. Wen, T.-C. Hou, Z. L. Wang, *Adv. Energy Mater.* **2013**, *3*, 1563.
[23] L. Lin, S. Wang, S. Niu, C. Liu, Y. Xie, Z. L. Wang, *ACS Appl. Mater. Interfaces* **2014**, *6*, 3031.
[24] Y. Xie, S. Wang, S. Niu, L. Lin, Q. Jing, Y. Su, Z. Wu, Z. L. Wang, *Nano Energy* **2014**, *6*, 129.
[25] G. Zhu, J. Chen, T. Zhang, Q. Jing, Z. L. Wang, *Nat. Commun.* **2014**, *5*, 3426.
[26] X. Fan, J. Chen, J. Yang, P. Bai, Z. Li, Z. L. Wang, *ACS Nano* **2015**, *9*, 4236.
[27] J. Yang, J. Chen, Y. Liu, W. Yang, Y. Su, Z. L. Wang, *ACS Nano* **2014**, *8*, 2649.
[28] V. Nguyen, R. Zhu, R. Yang, *Nano Energy* **2015**, *14*, 49.
[29] H. Zhang, Y. Yang, Y. Su, J. Chen, C. Hu, Z. Wu, Y. Liu, C. Ping Wong, Y. Bando, Z. L. Wang, *Nano Energy* **2013**, *2*, 693.
[30] Y. Hu, J. Yang, S. Niu, W. Wu, Z. L. Wang, *ACS Nano* **2014**, *8*, 7442.
[31] Y. Yang, H. Zhang, J. Chen, S. Lee, T.-C. Hou, Z. L. Wang, *Energy Environ. Sci.* **2013**, *6*, 1744.
[32] Y. Zi, L. Lin, J. Wang, S. Wang, J. Chen, X. Fan, P.-K. Yang, F. Yi, Z. L. Wang, *Adv. Mater.* **2015**, *27*, 2340.
[33] K. Zhang, X. Wang, Y. Yang, Z. L. Wang, *ACS Nano* **2015**, *9*, 3521.
[34] X. Zhong, Y. Yang, X. Wang, Z. L. Wang, *Nano Energy* **2015**, *13*, 771.
[35] H. Guo, J. Chen, Q. Leng, Y. Xi, M. Wang, X. He, C. Hu, *Nano Energy* **2015**, *12*, 626.
[36] H. Guo, Q. Leng, X. He, M. Wang, J. Chen, C. Hu, Y. Xi, *Adv. Energy Mater.* **2015**, *5*, 1400790.
[37] Z. Wen, J. Chen, M.-H. Yeh, H. Guo, Z. Li, X. Fan, T. Zhang, L. Zhu, Z. L. Wang, *Nano Energy* **2015**, *16*, 38.
[38] M.-H. Yeh, L. Lin, P.-K. Yang, Z. L. Wang, *ACS Nano* **2015**, *9*, 4757.
[39] T. Sudhawiyangkul, D. Isarakorn, *12th Int. Conf. Electrical Engineering/Electronics, Computer, Telecommunications and Information Technology (ECTI-CON), 2015*, IEEE, Hua Hin, Thailand **2015**, pp. 1–6.
[40] S. P. Beeby, R. Torah, M. Tudor, P. Glynne-Jones, T. O'Donnell, C. Saha, S. Roy, *J. Micromech. Microeng.* **2007**, *17*, 1257.
[41] C. Cepnik, O. Radler, S. Rosenbaum, T. Ströhla, U. Wallrabe, *Sens. Actuators A: Phys.* **2011**, *167*, 416.
[42] L.-D. Liao, P. C. Chao, J.-T. Chen, W.-D. Chen, W.-H. Hsu, C.-W. Chiu, C.-T. Lin, *Magn. IEEE Trans.* **2009**, *45*, 4621.
[43] G. Zhu, Y. S. Zhou, P. Bai, X. S. Meng, Q. Jing, J. Chen, Z. L. Wang, *Adv. Mater.* **2014**, *26*, 3788.
[44] D. P. Arnold, *Magn. IEEE Trans.* **2007**, *43*, 3940.
[45] H. Guo, J. Chen, L. Tian, Q. Leng, Y. Xi, C. Hu, *ACS Appl. Mater. Interfaces* **2014**, *6*, 17184.
[46] S. Wang, Y. Xie, S. Niu, L. Lin, Z. L. Wang, *Adv. Mater.* **2014**, *26*, 2818.
[47] S. Niu, Y. Liu, X. Chen, S. Wang, Y. S. Zhou, L. Lin, Y. Xie, Z. L. Wang, *Nano Energy* **2015**, *12*, 760.
[48] C. Zhang, W. Tang, C. Han, F. Fan, Z. L. Wang, *Adv. Mater.* **2014**, *26*, 3580.

